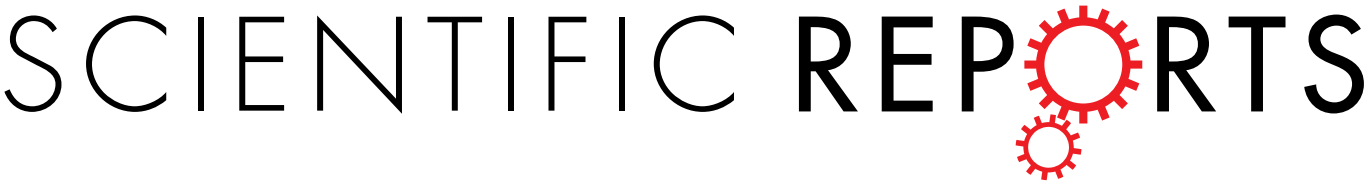

OPEN

Increasing the detection distance of remote NMR using wireless inductive coupling coil

Received: 18 May 2017
Accepted: 14 September 2017
Published online: 04 October 2017

Mario Henrique M. Killner[1,2], Giancarlo Tosin[3], André S. Carvalho[4], Diego Firme Bernardes[1] & Luiz Alberto Colnago[1]

Unilateral nuclear magnetic resonance (UNMR) spectrometers have been applied in a variety of fields such as petrochemistry, materials science, and process control[1]. In UNMR measurements the sample is placed outside of the UNMR sensor and the signal intensity is reduced almost exponentially as the sample-to-sensor distances increases. To expand the detection limits of remote UNMR sensors, wireless inductive coupling was proposed and tested. This strategy was proved to reduce signal attenuation due to sample detachment from sensor, resulting in an increase in detection distance by one order of magnitude (i.e., from few millimeters to few centimeters). This novel approach broadens the potential applications of UNMR sensors and opens new opportunities in several areas, from chemical to biomedical applications.

Nuclear magnetic resonance (NMR) spectroscopy and imaging have been among the most powerful analytical tools applied from atoms/molecules to large living organism, including human beings. Most of these applications are performed inside bulky and heavy magnets, being sample or organism dimensions restricted by the magnet's bore or gap[1]. In order to bypass this limitation, several magnet and probe designs (e.g., opposite field and single-sided or unilateral magnets) have been developed for remote NMR detection. In these systems, the analyses are performed outside of the sensor (remote detection) so that sample dimension is not a limiting factor[1]. The first commercial application of this principle was in the petroleum industry, in which remote NMR sensors denote a standard tool for well-logging procedures to estimate oil, gas, and moisture contents, reservoir porosity, and many other parameters related to porous media[3].

Encouraged by the use of permanent magnets, much smaller unilateral NMR sensors weighting few kilograms and accepting inhomogeneous and strong gradient fields for depth profile have been developed and used in the past two decades. These sensors first appeared in the scientific literature in 1995 along with the NMR-MOUSE[4], a mobile surface scanner based on two small permanent magnets mounted on a horseshoe geometry. Thereafter, different permanent magnet geometries have been developed in order to increase the depth sensitivity range of such unilateral sensors. These new NMR surface explorers and depth profiling have been used to analyze samples in various fields (e.g., chemistry, physics, archeology, human heritage, and biomedical, materials, and environmental sciences) in different measurements, including remote monitoring of chemical reactions, viscosity, porosity, diffusion through materials, painting authenticity, and diseases (e.g., cancer), among many other applications[4–8].

An inherent, unwanted characteristic of unilateral NMR (UNMR) devices is that the signal decays roughly exponentially with distance from sensor surface, limiting the detection distance to a few millimeters for small UNMR sensors. Numerous efforts have been proposed to increase the detection distance based on magnetic geometry[9,10] and/or coil arrangements[11]. In this study, we demonstrate a simple, efficient strategy to expand the detection limits of small UNMR sensors based on wireless inductive coupling sensor (coil and tuning capacitor). Inductive coupling coils have been used to enhance signal-to-noise ratio (SNR) in high-resolution solid-state NMR and magnetic resonance imaging[12–14]. This new configuration increases the detection limit by one order of magnitude, from a few millimeters to a few centimeters.

[1]Embrapa Instrumentação, Rua XV de Novembro 1452, São Carlos, SP, 13560-970, Brazil. [2]Universidade Estadual de Londrina, Pr 445–km 380, Londrina, PR, 86057-970, Brazil. [3]LMA Magnet Consultancy, Rua Filomeno Rispoli 509, 13564-200, São Carlos, São Paulo, Brazil. [4]Instituto de Química de Sao Carlos, Universidade de São Paulo, Av. Trabalhador São-carlense 400, São Carlos, SP, Brazil. Correspondence and requests for materials should be addressed to L.A.C. (email: luiz.colnago@embrapa.br)

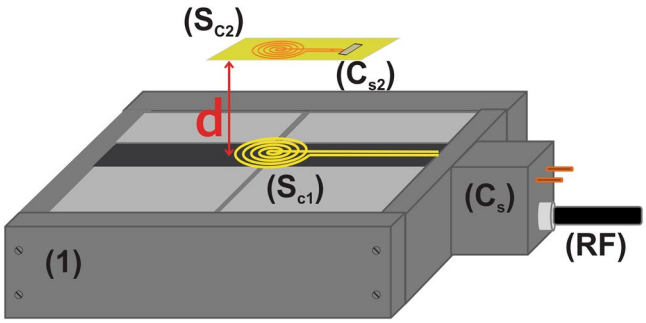

Figure 1. Apparatus used in this work, in which: (**1**) UNMR sensor; ($\mathbf{Sc_1}$) primary surface coil used on UNMR probe; ($\mathbf{Sc_2}$) secondary coil inductive coupled to $\mathbf{Sc_1}$ and located at a distance **d** from $\mathbf{Sc_1}$; ($\mathbf{C_s}$) aluminum box with the matching and tuning variable capacitors of $\mathbf{Sc_1}$ coil; ($\mathbf{C_{s2}}$) chip ceramic capacitor connected in shunt with $\mathbf{Sc_2}$; (**RF**) coaxial cable connecting the magnetic sensor to the spectrometer.

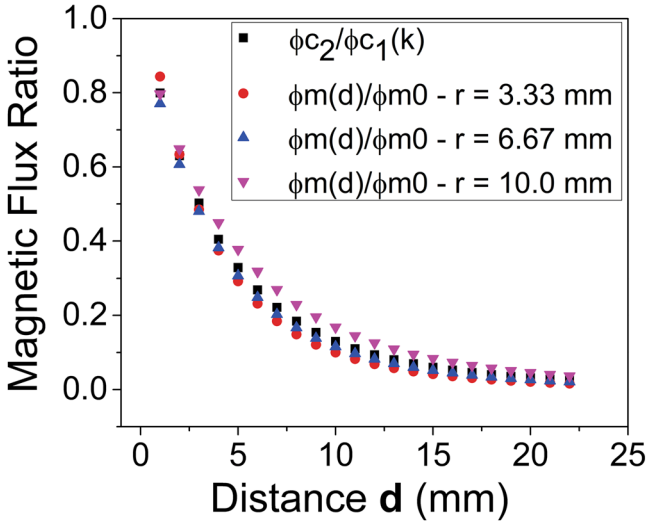

Figure 2. Magnetic Flux Ratio for three magnetized disks with different radii as well as the coupling (k) between the $\mathbf{S_{C1}}$ and $\mathbf{S_{C2}}$ coils.

Results

Secondary coil coupling to the unilateral NMR device. Fig. 1 illustrates the apparatus applied in this work. The secondary coil ($\mathbf{S_{c2}}$) is composed of a thin copper coil etched on a printed circuit board. This coil was tuned by soldering a chip capacitor onto it. The capacitor was chosen based on the primary coil frequency that maintained the so-called 'over coupling' regime wherein all the dissipated power in the primary coil is essentially dissipated in the secondary circuit. To reach as higher **SNR** values as possible, the coupled system was also matched to 50 Ω [12–15].

In a typical single-sided magnet, the coil is placed close to the magnet surface, as depicted by $\mathbf{S_{C1}}$ in Fig. 1. When the region to be analyzed is far from the $\mathbf{S_{C1}}$ coil, the signal induced by nuclear spin precession and relaxation usually has remarkably low intensity. A straightforward means of increasing signal intensity is by surrounding the sample region with a second coil $\mathbf{S_{C2}}$, which in turn is coupled by mutual-inductance to $\mathbf{S_{C1}}$.

Computational simulations were carried out using FEMM 4.2 software[Y20] in order to estimate the relative magnetic flux in the $\mathbf{S_{C1}}$ and $\mathbf{S_{C2}}$ coils generated by the nuclear spins. Thus, homogenously narrow disks with width similar to the diameters of coil wire, magnetized perpendicularly to the coil surface, were positioned concentrically to the coil axis. The magnetic flux perpendicular to the coil surface $\Phi_m(d)$ was then calculated as a function of the distance $\boldsymbol{d}$ from the coil to the magnetized region. Figure 2 presents $\Phi_m(d)$ normalized by the flux m^0, which corresponds to $\mathbf{d} = 0$ mm, for three different magnetized disk diameters: 6.7, 13.3 and 20 mm.

Although single-sided magnets do not feature a homogeneous circular region, calculations exploiting the code tridimensional feature provide an idea of the behavior of induced signal amplitude when only the primary coil ($\mathbf{S_{C1}}$) is used in the measurement. This decay is denoted by the function $f_m(\mathbf{d})$, which can be fitted exponentially. The amplitude of the induced voltage V_1 in the $\mathbf{S_{C1}}$ coil is thus given by $V^0{}_1 f_m(d)$, where in $V^0{}_1$ is V_1 at $d = 0$ mm. In other words, $f_m(\mathbf{d})$ directly shows the decay of the signal amplitude of $\mathbf{S_{C1}}$ coil in a circuit without the secondary coupling coil ($\mathbf{S_{C2}}$).

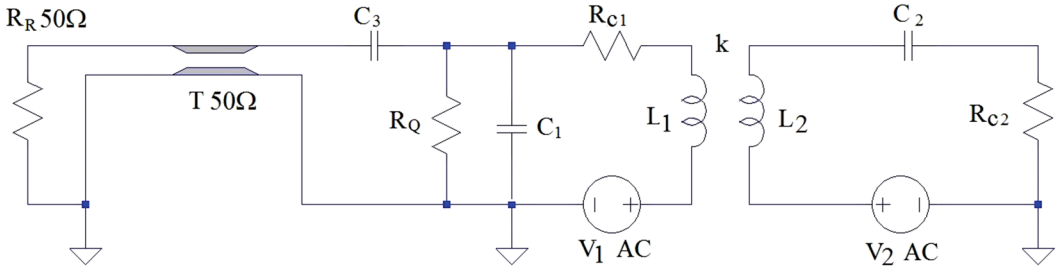

Figure 3. Electronic schematics applied for inductive coil coupling.

Coil coupling was also simulated using FEMM 4.2 software. In this situation, one coil was fed with a current of 1 Amp and the normal magnetic flux was assessed in the second one as a function of distance ***d***. Figure 2 presents the ratio (Φ_{12}/Φ_{11}) between the flux Φ_{12} created by coil $\mathbf{S_{C1}}$ in the coil $\mathbf{S_{C2}}$ as well as the flux Φ_{11}, generated by $\mathbf{S_{C1}}$ itself. The flux Φ_{12} is related to mutual inductance M_{12} and the ratio Φ_{12}/Φ_{11} is the coupling factor "k". The flux Φ_{11} corresponds to self-inductance L_1 or, for Φ_{22}, L_2. As $L_1 = L_2 = L$ in this study, $M_{12} = k\,(L_1.L_2)^{1/2} = k.L$. Because of the magnetic field linearity generated by these coils, the self-inductance is directly obtained when the current is set to 1 Amp.

Figure 2 also shows that the fluxes of magnetized disks decay like the flux created by one coil in the other one. This happens because the homogeneously magnetized disk can be replaced by the magnetization current density, what makes the magnetic field of the disk equals to that of a coil with one turn.

Circuitries for excitation/detection of coupling coil regarding both high and 50 Ω impedances may be found in the literature[15–18]. The circuits chosen in the experiment reported here are illustrated in Fig. 3. If one considers only the physically connected left side, it would be a common circuit typically used in NMR devices, applying tuning and matching capacitors (C_2 and C_3) as well as R_Q resistor for circuit quality factor (Q) adjustment. T means the coaxial cable (50 Ω) and the output voltage is on R_R. Rc indicates the resistances for both coils. The entire circuit was then used for inductive coupling. It also consisted of capacitors for impedance matching and resonance frequency tuning.

Since the voltage induced in the coil $\mathbf{S_{C1}}$ is not negligible, the voltage source V_1 was included in the circuit topology in addition to V_2, which is induced in the coil $\mathbf{S_{C2}}$. These circuits were analyzed through *LTspice* code[19]. Although there was not a rigorous modeling taking into account the exact coil geometries, copper shielding, the ferromagnetic influence of the carbon steel base magnet, and the dynamic analyses, the gains associated to coupled coil signal and its quasi-constant behavior could be seen.

If the sub-circuit that contains the $\mathbf{S_{C1}}$ coil has a high impedance, as the $\mathbf{S_{C1}}$ coil terminals are open, the tuning is obtained by $\mathbf{C_2}$ capacitor and the mutual inductance does not influence the current in the coupled circuit. The maximum current I_2 is given by V_2/R_2 at the resonance frequency (w_r). In this situation, the voltage between the $\mathbf{S_{C1}}$ coil terminals (V_{0c}) is then the voltage of the coupled coils subtracting the voltage directly induced by the nuclear spins in $\mathbf{S_{C1}}$, since they produce opposite magnetic fluxes. Thus, V_{0c} can be expressed by Eq. 1.

$$V_{0c} = Mw_r\frac{V_2}{R_2} - f_m(d)V_2 = \left[\frac{Lkw_r}{R_2} - f_m(d)\right]V_2 \tag{1}$$

On the other hand, the voltage V_0 of the uncoupled circuit is obtained by Eq. 2 and the gain is the ratio V_{0c}/V_0.

$$V_0 = -f_m(d)V_2 \tag{2}$$

Intensity of the NMR signal versus sample distance (d) from the sensor. To evaluate the improvement of signal intensity due to the implementation of a secondary inductive coil coupled to the UNMR sensor, NMR spin echoes of a thin automotive lubricant oil layer were recorded at different distances **d** from the sensor surface using surface coil and the wireless inductive coupled coil. **d** was varied through the sequential addition of microscopy glass sliders (1 mm in thickness) between the sensor and the sample. It is worth mentioning that, for the inductive coupled experiments, **d** reflects the distance between $\mathbf{Sc_1}$ and $\mathbf{Sc_2}$ coils, being the sample positioned right above the $\mathbf{Sc_2}$ coil. Figure 4 shows the maximum intensities of the NMR echoes recorded at different distances **d**.

As evidenced in Fig. 4, the intensities of the NMR signals using the surface coil $\mathbf{Sc_1}$ (squares) and the remote coil $\mathbf{Sc_2}$ (circles) are remarkably different at distances from the sensor higher than 2 mm. At approximately 6 mm, the signal resulting from $\mathbf{Sc_1}$ was within the detection limit and presented a SNR equal to 3, whereas the intensity measured at the same distance with $\mathbf{Sc_2}$ was identical do the $\mathbf{Sc_1}$ on the surface. The intensity of the signal at 20 mm using the wireless remote coil was equal to that at 2 mm using the surface coil. This is equivalent to a one order of magnitude enhancement in signal intensity, indicating the greater advantage of this coupling. Although this advantage is not universal, we can envisage numerous applications for the wireless remote inductive coupled coil, which can boost the use of remote NMR.

Monitoring plaster curing. The secondary coil was also used to monitor the curing process of plaster. Figure 5a shows the evolution of the maximum signal intensity of the first echo, while Fig. 5b presents the

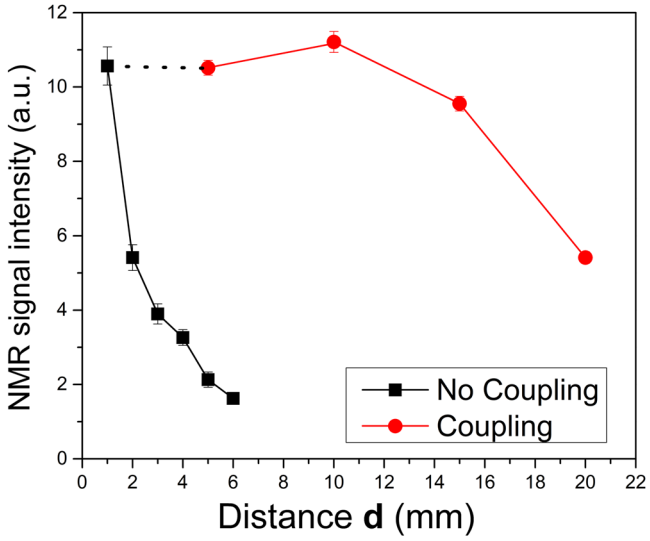

Figure 4. Maximum spin-echoes intensities at different distances **d** between the oil sample and the $\mathbf{S_{C1}}$ coil using the inductive coupled $\mathbf{S_{C2}}$ coil (red circles) and only $\mathbf{S_{C1}}$ coil (black squares).

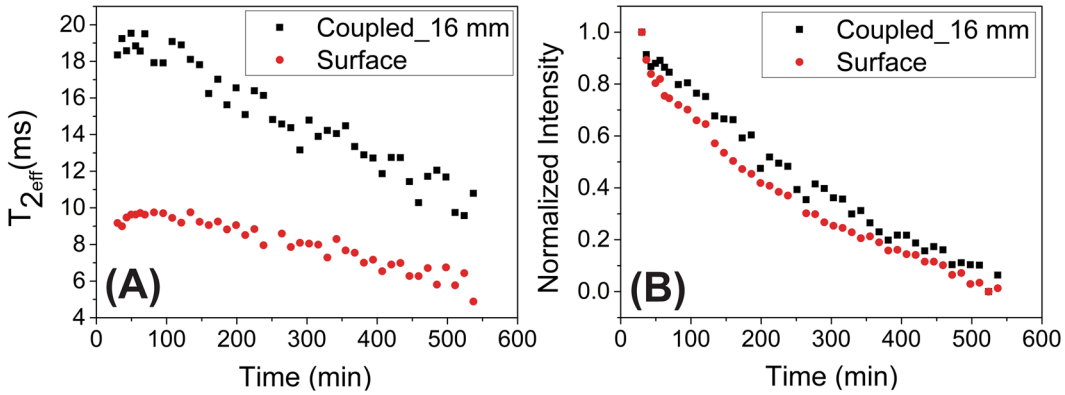

Figure 5. Evolution of the NMR signal acquired by CPMG pulse sequence during plaster curing. (**A**) is the determined T_{2eff} and (**B**) is the normalized maximum intensity of the first CPMG echo. Both data are plotted over curing time. The squares are data from the inductive coupling of $\mathbf{S_{c2}}$ (embedded in the plaster cube and located 16 mm from the NMR sensor surface), while the circles are data from the common set-up (sample located close to the sensor surface, with $\mathbf{d} = 2$ mm).

behavior of effective transverse relaxation time ($\mathbf{T_{2eff}}$) recorded by the CPMG pulse sequence of a plaster block ($40 \times 40 \times 35\,mm^3$) as a function of curing time. The circles denote the measurements made 2 mm away from the sensor surface ($\mathbf{d} = 2$ mm) using only the primary coil. The squares are measurements made using the secondary coil embedded in the plaster cube as well as inductive coupled to the primary coil. It was located 16 mm from the magnet surface.

Even though discussing mass transport and water mobility (curing process) on a time course in not the goal of this work, one may observe in Fig. 5b that the signal intensity related to water content decays faster on the surface than in the center of the plaster block. The difference between such positions was not larger because the glass sliders used to protect the $\mathbf{S_{c1}}$ coil limited water evaporation. Water loss during the experiments was approximately 25%.

Larger differences between $\mathbf{T_{2eff}}$ were observed in the two positions (Fig. 5b). The lower $\mathbf{T_{2eff}}$ values on the surface can be explained by fast decay of CPMG signal caused by water diffusion in the presence of larger magnetic field inhomogeneity at the magnet surface[4]. At 16 mm, the magnetic field inhomogeneity is smaller than on the magnet surface and the effect of water diffusion is less pronounced. The smaller decay of $\mathbf{T_{2eff}}$ values on the surface than at 16 mm can be explained by the reduced water diffusion due to hydration process that takes place concomitantly to water evaporation[20].

Discussion

In summary, a simple, efficient means of enhancing the detection distance of small UNMR sensors based on wireless inductive coupling sensor, involving neither coils featuring sophisticated designs nor larger magnets and

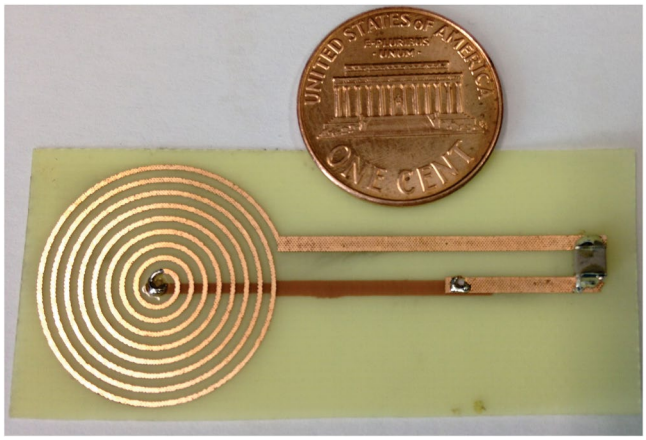

Figure 6. Secondary coil built on a double-sided coppered printed circuit board. A penny is shown for size comparison. The chip ceramic capacitor soldered to the coil can be seen on the right-end edge.

coils, was demonstrated. The proposed configurations increased the detection distance by more than one order of magnitude, opening new opportunities for field applications of UNMR sensor. Although this advantage is not universal, several applications of the wireless remote inductive coupled coil may be envisaged, boosting the use of remote NMR. Some potential applications are listed below:

a) Monitoring chemical reactions that need to be isolated from the NMR sensor. The remote wireless sensor can also be applied to reduce the effect of magnetic field on electrochemical reactions[21], as the electrochemical cell can be positioned in an area of low magnetic field.
b) Biomedical applications, in which the $\mathbf{Sc_2}$ coils could be applied as bandages on specific regions of the body to evaluate the evolution of bone or soft tissue lesions caused by traumatic and infectious processes or even tumoral lesions.
c) Materials Engineering, to monitor polymerization reactions either in laboratory or pilot scales as well as in manufactured products. Civil Engineering, to monitor curing and degradation processes of cement. In the latter, embedding $\mathbf{Sc_2}$ coils into a concrete structure could provide valuable internal chemical and physical information concerning the sample.

Moreover, the simple $\mathbf{S_{C2}}$ design, built on the thin-coppered print circuit board, keeps the instrumentation costs low, which creates the possibility to make disposable coils depending upon the application.

Methods

Home-built UNMR sensor. A more detailed description of the UNMR sensor construction can be found elsewhere[22]. Basically, it was built using four axially magnetized NdFeB alloy blocks ($2.54 \times 2.54 \times 1.27\ cm^3$) mounted on a carbon steel yoke base. Each pole was constructed with two blocks with the same orientation and separated by a 2-mm gap. The separation between the two poles was 14 mm[6,22,23]. The coil probe ($\mathbf{Sc_1}$) was built in 20 awg copper wire with 9 turns and having an external diameter equal to 20 mm. Matching and tuning variable capacitors (**Cs**) ranging from 5 to 25 pf and from 5 to 50 pf, respectively, were used to adjust the probe between 25.550 MHz (0.6 T on sensor surface) and 10.650 MHz (0.25 T, 20 mm above sensor surface), where the system showed Q values around 50. For frequencies lower than 24.000 MHz, chip ceramic capacitors up to 300 pf were added in parallel to tune the circuit at the desired frequency. The UNMR sensor was connected to a NMR console CAT-100 (*Tecmag*, Houston, USA), a 3205 AMT power amplifier, and an AU 1114 preamplifier.

Secondary coil fabrication. The wireless remote coil $\mathbf{Sc_2}$ was etched in a 0.2-mm thick, double-sided, coppered printed circuit board ($55 \times 25\ mm^2$). The resonance circuit was tuned to each frequency by a specific chip ceramic capacitor ($\mathbf{C_{s2}}$). The $\mathbf{S_{C2}}$ coil had 9 turns with an external diameter of 20 mm. As previously stated, the chip capacitor soldered to it was intended to keep the coupled system working on the over coupling regime, *e.g.* for 11.010 MHz at 20 mm, whereas the primary coil was set at 10.912 MHz, the secondary coil was set at 11.287 MHz. Figure 6 shows a picture of the secondary coil.

NMR experiments. The intensities of the NMR echo signals were acquired using a spin echo sequence with 2-μs-long RF pulses separated by a time τ of 512 μs and averaged with 200 scans. The intensities of the echo signals were measured with an automotive lubricant oil sample (0.5-mm-thick layer). For the analyses without the remote coil, the sample distance to the sensor varied up to 6 mm, while for the remote coil it ranged up to 20 mm. CPMG pulse sequence was used to monitor the plaster curing process using 2-μs-long RF pulses separated by a time τ of 500 μs, 1200 refocusing pulses, and an average of 300 scans.

Plaster curing experiment. The plaster was bought in a neighborhood market as plaster of Paris powder. It was previously prepared in a beaker by mixing powder and tap water at a 1:0.8 weight ratio. Then, it was

transferred to an acrylic box of $40 \times 40 \times 35\,mm^3$ (l x w x h) with a 1-mm glass slider at the bottle, for molding and setting on the UNMR sensor. To monitor the curing process on the surface, a sample of freshly prepared plaster was placed on the surface of the $\mathbf{Sc_1}$ coil. For remote analyses, the $\mathbf{Sc_2}$ coil was embedded in the center of the plaster. Subsequently, 43 CPMG experiments were performed during 9 hours. To accelerate the curing process, a fan was placed 50 cm away from the experimental set-up and the room temperature was maintained at $25 \pm 1\,°C$.

References

1. Blümich, B., Perlo, J. & Casanova, F. Mobile single-sided NMR. *Prog. Nucl. Mag. Res. Sp.* **52**, 197 (2008).
2. Yamauchi, K., Janssen, J. W. G. & Kentgens, A. P. M. Implementing solenoid microcoils for wide-line solid-state NMR. *J. Magn. Reson.* **167**, 87 (2004).
3. Brown, R. J. S. *et al*. PART 1: Earth's-field nuclear magnetic logging. *Concept. Magnetic Res.* **13**, 340 (2001).
4. Eidmann, G., Savelsberg, R., Blümer, P. & Blümich, B. The NMR mouse, a mobile universal surface explorer. *J. Magn. Reson. Ser. A* **122**, 104 (1996).
5. Casanova, F., Perlo, J., Blümich, B. (Eds.) Single-sided NMR Ch.1 & 4 (Springer 2011).
6. Perlo, J., Casanova, F. & Blümich, B. Profiles with microscopic resolution by single-sided NMR. *J. Magn. Reson.* **176**, 64 (2005).
7. Oligschläger, D. *et al*. A miniaturized NMR-mouse with a high magnetic field gradient (mini-mouse). *Appl. Magn. Reson.* **46**, 181 (2015).
8. Dalitz, F., Cudaj, M., Maiwald, M. & Guthausen, G. Process and reaction monitoring by low-field NMR spectroscopy. *Prog. Nucl. Mag. Res. Sp.* **60**, 52 (2012).
9. Marble, A. E., Mastikhin, I. V., Colpitts, B. G. & Balcom, B. J. An analytical methodology for magnetic field control in unilateral NMR. *J. Magn. Reson.* **174**, 78 (2005).
10. McDonald, P. J., Aptaker, P. S., Mitchell, J. & Mulheron, M. A unilateral NMR magnet for sub-structure analysis in the built environment: the surface GARField. *J. Magn. Reson.* **185**, 1 (2007).
11. Oligschläger, D. *et al*. Miniaturized multi-coil arrays for functional planar imaging with a single-sided NMR sensor. *J. Magn. Reson.* **254**, 10 (2015).
12. Sakellariou, D., Le Goff, G. & Jacquinot, J.-F. High-resolution, high-sensitivity NMR of nanolitre anisotropic samples by coil spinning. *Nature* **447**, 694 (2007).
13. Koo, C. *et al*. A microfluidically cryocooled spiral microcoil with inductive coupling for MRmicroscopy. *IEEE T. Bio-Med. Eng.* **61**, 76 (2014).
14. Terman, F. E. Electronic and radio engineering Ch. 3 (McGraw-Hill 1955).
15. Jacquinot, J.-F. & Sakellariou, D. NMR signal detection using inductive coupling: applications to rotating microcoils. *Concept. Magnetic Res. A* **38A**, 33 (2011).
16. Decorps, M., Blondet, P., Reutenauer, H., Albrand, J. P. & Remy, C. An inductively coupled, series-tuned NMR probe. *J. Magn. Reson.* **65**, 100 (1985).
17. Kuhns, P. L., Lizak, M. J., Sam-Hyeon, L. & Conradi, M. S. Inductive coupling and tuning in NMR probes: applications. *J. Magn. Reson.* **78**, 69 (1988).
18. Raad, A. & Darrasse, L. Optimization of NMR receiver bandwidth by inductive coupling. *Magn. Reson. Imaging* **10**, 55 (1992).
19. LTspice code, website: http://www.linear.com/ltspice (2017).
20. Cano-Barrita, P. F. & de, J. *et al*. Embedded NMR sensors to monitor evaporable water loss caused by hydration and drying in Portland cement mortar. *Cement Concrete Res.* **39**, 324 (2009).
21. Gomes, B. F., Nunes, L. M. S., Lobo, M. S. L., Cabeça, L. F. & Colnago, L. A. *In situ* study of the magnetoelectrolysis phenomenon during copper electrodeposition using time domain NMR relaxometry. *Anal. Chem.* **86**, 9391 (2014).
22. Cabeça, L. F., Marconcini, L. V., Mambrini, G. P., Azeredo, R. B. V. & Colnago, L. A. Monitoring the transesterification reaction used in biodiesel production, with a low cost unilateral nuclear magnetic resonance sensor. *Energ. Fuel* **25**, 2696 (2011).
23. Blümich, B., Casanova, F., Perlo, J. Single-sided NMR sensor with microscopic depth resolution US PATENT, Pub. N°: US 7, 358, 734 B2 April 15th, 2008.

Acknowledgements

We thank the São Paulo Research Foundation (FAPESP) grants numbers 2013/25802-2, 2014/22126-9 and 2017/12864-0 and CNPq grant 303837/2013-6 for financial support.

Author Contributions

L.A. Colnago and M.H.M Killner conceived the experiment, drafted the manuscript, and reviewed its text and figures. G. Tosin performed computer simulations, theoretical analyses, and drafted and reviewed the manuscript. A.S. Carvalho and D.F. Bernardes fabricated the devices and carried out the experiments.

Additional Information

Competing Interests: The authors declare that they have no competing interests.

Publisher's note: Springer Nature remains neutral with regard to jurisdictional claims in published maps and institutional affiliations.